# Intrapulse quantum spectral correlation of femtosecond optical pulses in optical fiber

Heongkyu Ju*
*Department of Physics, Gachon University, Gyeonggi-do, Korea, and*
*Gachon Bionano Research Institute, Gachon University, Gyeonggi-do, Korea*
(Received 26 September 2011; published 14 March 2012)

Intrapulse quantum spectral correlation of photon numbers of a femtosecond optical pulse, which propagates a 5-m-long optical fiber, is presented in a matrix format for quantum noise study by numerical calculation. The calculation includes the higher-order optical effects such as intrapulse-stimulated Raman scattering and self-steepening effects, as well as self-phase modulation and group velocity dispersion. The quantum correlations between spectral components (spectral resolution of 0.7 nm) which evolve with the pulse energy are provided in a matrix format at soliton orders including the low orders, $N = 0.1$ to 1.0 (a 0.1 step), to give the detailed properties of spectral correlation evolutions in the matrix format. It is shown that the photon-number correlations between spectral components near the pulse spectrum center form strong correlations of a square shape in the matrix, at a soliton order $N$ ($\leqslant 0.4$), and then are redistributed into those between spectral components near the spectrum wings such that the cross-shaped correlation pattern in the matrix begin to be visible at $N = 0.5$ before their further redistribution as $N \rightarrow 1.0$. In addition, significant anticorrelations can be increasingly extended to be found between spectral components near the spectrum center as $N \rightarrow 1.0$, leading to the expectation that the degree of photon-number squeezing by spectral filtering for subsolitons can be lower than that for solitons. Intrapulse-stimulated Raman scattering that starts to become visible at around $N = 0.6$ produces an asymmetric correlation structure with respect to the spectrum center in the correlation matrices while the relevant pulse self-frequency shift becomes visible at $N \geqslant 0.8$. The calculation presented indicates that the measurement of nonlinear effects which are not detectable distinctly at the classical level is possible at the quantum level.

DOI: 10.1103/PhysRevA.85.033810 PACS number(s): 42.65.Re, 42.50.Ar, 42.65.Tg, 42.50.Lc

## I. INTRODUCTION

Quantum spectral correlations of light propagating in a nonlinear media have been studied for the internal structure of light quantum noise [1–8]. In particular, the spectral correlations of photon numbers of an optical soliton have been observed experimentally at a soliton energy level [8], producing the quantum spectral correlation matrix where strong correlations were found between spectral components near the pulse spectrum wings. The intrapulse-stimulated Raman scattering has also been studied for quantum correlation of a fiber optical soliton [9,10] and those of light propagating microstructure fibers [11,12]. This correlation information can help us to understand quantum noise spectral structures of ultrafast optical pulses at the soliton energy level, and it helps to enhance photon-number squeezing by spectral filtering of ultrafast optical solitons where spectral correlations are redistributed by nonlinear optical effects such as self-phase modulation (SPM) and Raman scattering [3,5,7].

This paper presents, by numerical calculation, the spectral correlations of photon numbers of a 130-fs optical pulse propagating an optical fiber of 5 m in length, to show the evolution of an intrapulse quantum spectral structure with a pulse energy at soliton orders including low orders, that is, $N = 0.1$ to 1.0 (a 0.1 step). A beam propagation method with a linearization approximation is utilized for the calculation of quantum noise propagation [13,14] to present the intrapulse quantum spectral correlation matrices, with a spectral resolution of 0.7 nm. This can be expected to give more detailed properties about quantum correlation between spectral components than the case of investigating the photon-number variance (squeezing degree) under a spectrally integrated passband filter [5,6], for soliton orders from 0.1 to 1.0. The higher-order nonlinear optical effects such as intrapulse-stimulated Raman scattering and pulse self-steepening effects are included in the calculation.

It is shown that the intrapulse quantum spectral correlation properties evolve with increasing an incident pulse energy owing to nonlinear effects such as SPM and Raman scattering. However, for all soliton orders used in the calculation, the pulse self-steepening effects have a negligible impact on the quantum spectral correlation structure.

At $N \leqslant 0.4$, major correlations are visible between spectral components at around the pulse spectrum center, leading to the square-shaped correlation patterns in the matrices when the pulse energies are low enough to yield little spectrum changes at the fiber output. The evolution of quantum spectral correlations in the matrices with the pulse energy is visible due to the nonlinear effects which, however, yield small spectrum changes at $N \leqslant 0.3$.

As $N$ increases from 0.5 to 0.8, the cross-shaped correlations in the matrices begin to grow, indicating that the phase transition of internal quantum noise structure occurs at around $N = 0.5$, as similarly found in Refs. [5,6]. With increasing the pulse energy toward the fundamental soliton threshold, significant anticorrelations are, however, found between spectral components near the pulse spectrum center, with the redistribution of correlations into those between the spectral components near the spectrum wings. This indicates that nonlinear spectral filtering produces the photon-number squeezing degrees for the fundamental soliton, which are higher than those for the subsoliton cases [15].

*http://gbri.kyungwon.ac.kr/home/?mode=faculty; batu@gachon.ac.kr

 

The significant asymmetric features with respect to the pulse spectrum center in the correlation matrix begin to be found at a soliton order of about $N = 0.7$, despite the fact that the substantial pulse spectrum asymmetry appears to be visible at $N \geqslant 0.9$. This is attributed to intrapulse-stimulated Raman scattering and implies that the higher-order nonlinear effects, which are difficult to observe at the classical level, can be detected at the quantum level [4]. This indicates that the evolution of quantum spectral correlation with the pulse energy leads to the possibility that nonlinear effects can be measured at the quantum level, even though their classical level detection is indistinct.

## II. QUANTUM NOISE CALCULATION

A 130-fs sech$^2$ optical pulse of a spectrum center of 1.5 $\mu$m is assumed to propagate along a single mode optical fiber of 5 m in length for calculation. The modeling of the propagation of a femtosecond pulse envelop and quantum noise includes higher-order nonlinear effects, such as intrapulse-stimulated Raman scattering, which are non-negligible in the subpicosecond regime. Thus, we use the extended quantum nonlinear Schrödinger equation for the pulse envelop operator $\hat{A}$ with a carrier frequency $\omega_0$ in the co-moving frame [16], as given by

$$\frac{\partial \hat{A}(z,t)}{\partial z} = -\frac{i}{2}\beta_2\frac{\partial^2}{\partial t^2}\hat{A} + \frac{i}{6}\beta_3\frac{\partial^3}{\partial t^3}\hat{A} + i\gamma\hat{A}^\dagger\hat{A}\hat{A} - \frac{\gamma}{\omega_0}\frac{\partial}{\partial t}[\hat{A}^\dagger\hat{A}\hat{A}] - i\gamma T_R\hat{A}\frac{\partial}{\partial t}[\hat{A}^\dagger\hat{A}], \quad (1)$$

where $\beta_2$ and $\beta_3$ are the parameters for the second- and the third-order group velocity dispersion (GVD), respectively. Here the third term on the right-hand side of Eq. (1) represents the SPM effects with $\gamma$ being the SPM coefficient while the fourth term describes the self-steepening effects which are caused by the intensity dependence of the group velocity [17]. The last term represents the intrapulse-stimulated Raman scattering with $T_R$ being the relevant parameter. Among all the terms on the right-hand side of Eq. (1), the first term (the second-order GVD) and the third term (SPM) are dominant, while the other terms have non-negligible effects on the propagation.

To obtain the equations for propagation of a classical pulse envelop and its counterpart quantum noise, let us employ a linearization approximation [13,14], i.e.,

$$\hat{A}(z,t) = A(z,t) + \hat{\delta}(z,t), \quad (2)$$

where $A(z,t)$ is the classical pulse envelop while $\hat{\delta}(z,t)$ is the quantum noise operator. Substituting Eq. (2) into Eq. (1) leads to

$$\frac{\partial\hat{\delta}}{\partial z} = \frac{i}{2}\beta_2F^{-1}[(\Delta\omega)^2F(\hat{\delta})] + \frac{i}{6}\beta_3F^{-1}[(\Delta\omega)^3F(\hat{\delta})] + i\gamma[2|A|^2\hat{\delta} + A^2\hat{\delta}^\dagger] - \gamma T_RAF^{-1} \times [(\Delta\omega)F(A^*\hat{\delta} + \hat{\delta}^\dagger A)] - \gamma T_R\hat{\delta}F^{-1}[(\Delta\omega)F(|A|^2)] + i\frac{\gamma}{\omega_0}F^{-1}[(\Delta\omega)F(2|A|^2\hat{\delta} + A^2\hat{\delta}^\dagger)], \quad (3)$$

where $F$ and $F^{-1}$ denote the Fourier and the inverse Fourier transformations, respectively. For calculation, the temporal pulse profile should be divided into a sufficient number of time bins, while the whole temporal window of calculation, which is much longer than the pulse period, must be ensured to be broad enough to minimize the computation error for calculating terms including $(\Delta\omega)^k$, where $k = 1$ and 2, in the femtosecond regime. Note that the other terms, except the SPM term (the third term), on the right-hand side of Eq. (3) induce couplings between the different time bins. Consequently, the quantum noise operator can be expanded by a linear combination of annihilation and creation operators $\hat{a}$ and $\hat{a}^\dagger$ of an input vacuum field [13,14], as given by

$$\hat{\delta}_p(n) = \sum_q \mu_{pq}(n)\hat{a} + \nu_{pq}(n)\hat{a}^\dagger, \quad (4)$$

where $p$ and $q$ are the time indices while $n$ is the distance index. The coefficient matrices $\mu_{pq}$ and $\nu_{pq}$ are obtained by substituting Eq. (4) into Eq. (3). After some algebra with the commutation relation between $\hat{a}$ and $\hat{a}^\dagger$, the equations for propagation of coefficient matrices are given as follows:

$$\mu_{pq}(n+1) = \mu_{pq}(n) + \frac{i}{2}\beta_2F_D^{-1}[(\Delta\omega)^2F_D(\mu_{sq}(n))]_p\Delta z + \frac{i}{6}\beta_3F_D^{-1}[(\Delta\omega)^3F_D(\mu_{sq}(n))]_p\Delta z + 2i\gamma|A_p(n)|^2\mu_{pq}(n)\Delta z + i\gamma A_p^2(n)\nu^*_{pq}(n)\Delta z - \gamma T_RA_p(n)F_D^{-1}[\Delta\omega F_D(A^*(n)\mu_{sq}(n) + A(n)\nu^*_{sq}(n))]_p\Delta z - \gamma T_R\mu_{pq}(n)F_D^{-1}[(\Delta\omega)F_D(|A(n)|^2)]_p\Delta z - i\frac{\gamma}{\omega_0}F_D^{-1}[\Delta\omega F_D(2|A(n)|^2\mu_{sq}(n) + A^2(n)\nu^*_{sq}(n))]_p\Delta z, \quad (5)$$

$$\nu_{pq}(n+1) = \nu_{pq}(n) + \frac{i}{2}\beta_2F_D^{-1}[(\Delta\omega)^2F_D(\nu_{sq}(n))]_p\Delta z + \frac{i}{6}\beta_3F_D^{-1}[(\Delta\omega)^3F_D(\nu_{sq}(n))]_p\Delta z + 2i\gamma|A_p(n)|^2\nu_{pq}(n)\Delta z + i\gamma A_p^2(n)\mu^*_{pq}(n)\Delta z - \gamma T_RA_p(n)F_D^{-1}[\Delta\omega F_D(A(n)^*(n)\nu_{sq}(n) + A(n)\mu^*_{sq}(n))]_p\Delta z - \gamma T_R\nu_{pq}F_D^{-1}[\Delta\omega F_D(|A(n)|^2)]_p\Delta z - i\frac{\gamma}{\omega_0}F_D^{-1}[\Delta\omega F_D(2|A(n)|^2\nu_{sq}(n) + A^2(n)\mu^*_{sq}(n))]_p\Delta z. \quad (6)$$

Here $F_D$ and $F_D^{-1}$ denote the discrete Fourier and inverse Fourier transformations, respectively. The coefficient matrices obtained by Eqs. (5) and (6) are two-dimensional Fourier-transformed into the spectral domain to calculate the photon-number covariance between the $i$th and the $j$th spectral components of the optical pulse, which is defined by

$$(\Delta\hat{\bar{n}})^2_{ij} \equiv \langle\hat{\bar{n}}_i\hat{\bar{n}}_j\rangle - \langle\hat{\bar{n}}_i\rangle\langle\hat{\bar{n}}_j\rangle. \quad (7)$$

Here $\hat{\bar{n}}_i$ is the photon-number operator for the $i$th spectral component and is defined by

$$\hat{\bar{n}}_i \equiv \hat{\bar{A}}_i^{\dagger} \hat{\bar{A}}_i, \tag{8}$$

where $\hat{\bar{A}}_i$ is the amplitude operator for the spectral component $i$.

For checking the calculation validity, the equations above are used to calculate the correlation matrix for a fundamental soliton (pulse energy of 54 pJ) propagating an optical fiber of 2.7 m in length using the optical parameters found in Refs. [7,8], which is compared with that experimentally obtained [8]. The similar pattern of the strong correlations between long-wavelength spectrum components, which contributes to the asymmetry of the matrix structure with respect to the matrix center, is produced while the similar anticorrelations between spectral components just shorter than the central wavelength and long-wavelength components are obtained, showing a qualitative agreement with the measurement.

Meanwhile, the optical parameters used in the calculation of the spectral correlation matrices presented below are $\beta_2 \approx -10.5$ ps$^2$/km [5,15], $\beta_3 \approx 0.1$ ps$^3$/km [15], and $n_2 \approx 3$ [5,15], where $\gamma \equiv \omega n_2/(cA_{\text{eff}})$ ($A_{\text{eff}}$ is an effective cross-sectional area for the third-order optical effects), and $T_R \approx 11$ fs [15].

## III. RESULT AND DISCUSSION

Figures 1(a)–1(j) show the pulse intensity profiles at the fiber output in the spectral domain for the soliton orders $N = 0.1$ to 1.0 (a 0.1 step), where the respective quantum spectral correlations are calculated. At the soliton orders $N = 0.1$ to 0.4, little change of the output pulse spectra from the input pulse spectrum (dashed lines) is shown, meaning implicitly the broadening of the pulse temporal length by dominance of GVD over SPM. However, The pulse spectrum narrowing starts to be seen approximately at around $N = 0.5$ and becomes significant at the soliton order of about $N = 0.8$, due to the increasing SPM effects that interplay with the GVD effects. The spectrum gets rebroadened at $N = 0.9$ and its width becomes close to the input pulse spectrum at $N = 1.0$ (pulse energy of about 54 pJ) with the self-frequency shift of the pulse spectrum center to about 1508 nm, which is induced by the intrapulse-stimulated Raman scattering [16].

Given the pulse spectrum evolution with the pulse energies, let us focus on the evolution of quantum spectral correlations which are normalized by

$$\mathrm{C}(i,j) \equiv \frac{(\Delta\hat{\bar{n}})_{ij}^2}{\sqrt{(\Delta\hat{\bar{n}})_{ii}^2 (\Delta\hat{\bar{n}})_{jj}^2}}. \tag{9}$$

Figures 2(a)–2(j) show the normalized correlation matrices at the soliton orders ranging from $N = 0.1$ to 1.0 with the incremental step of 0.1. In the case of $N = 0.1$ where the nonlinear effects such as SPM impose the little changes on the pulse spectrum, strong correlations are found between spectral components near the spectrum center, as shown in Fig. 2(a). They form a square around a center in the correlation matrix, which corresponds to the pulse spectral regions of significant intensity. As illustrated in Figs. 2(b)–2(d), raising

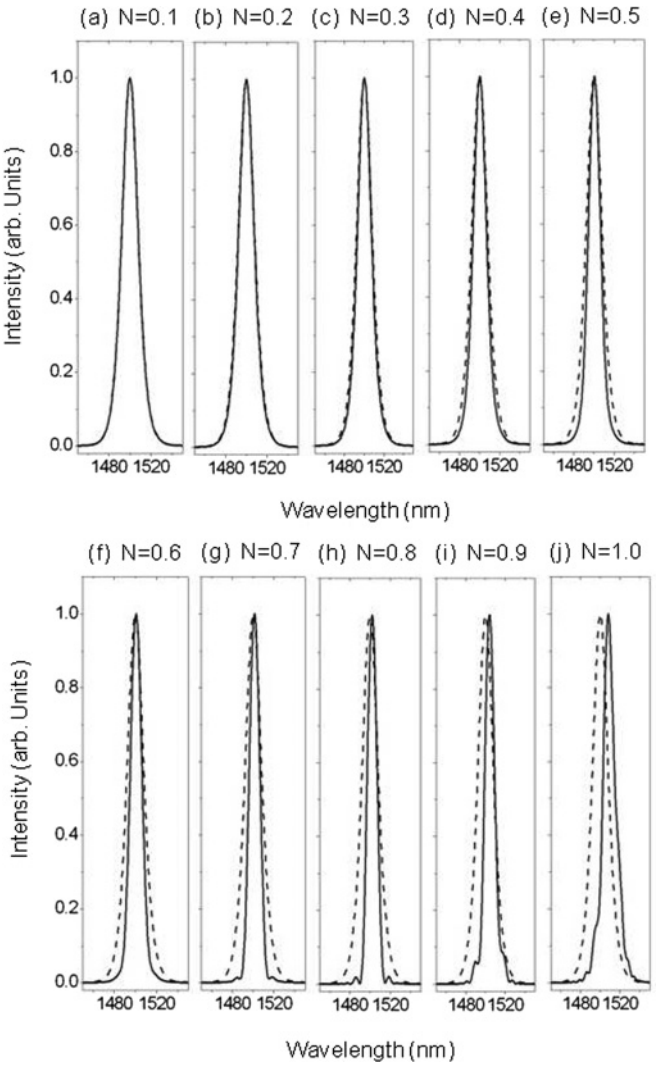


FIG. 1. Normalized output spectra (solid line) at the fiber output with the input pulse spectrum (dashed line) for soliton orders from $N = 0.1$ to 1.0.

the soliton order up to 0.4 does not substantially change the square pattern around the matrix center, while the contrast between correlations of the square and anticorrelations around it becomes low as $N \to 0.4$, indicating the redistribution of correlation induced by nonlinear effects, subject to the conservation of photon-number noise (variance) of the whole pulse spectrum. Despite little spectrum changes, the correlation changes induced by nonlinear effects such as SPM are shown to be visible as $N$ increases from 0.1 to 0.3. However, the square-shaped correlations are maintained as major correlations in the matrices as $N \leqslant 0.4$, implying that no significant phase transition in the quantum spectral structure occurs for these low soliton orders.

Figures 2(e)–2(g) show that the X-shaped cross-diagonal strong correlation pattern grows gradually as $N$ increases from 0.5 to 0.8, indicating that the start of the phase transition of the internal structure of the quantum correlation becomes visible at around $N = 0.5$, as similarly found in Refs. [5,6] where spectrally integrated photon-number variance is investigated under a spectral passband filter. The contrast between the black

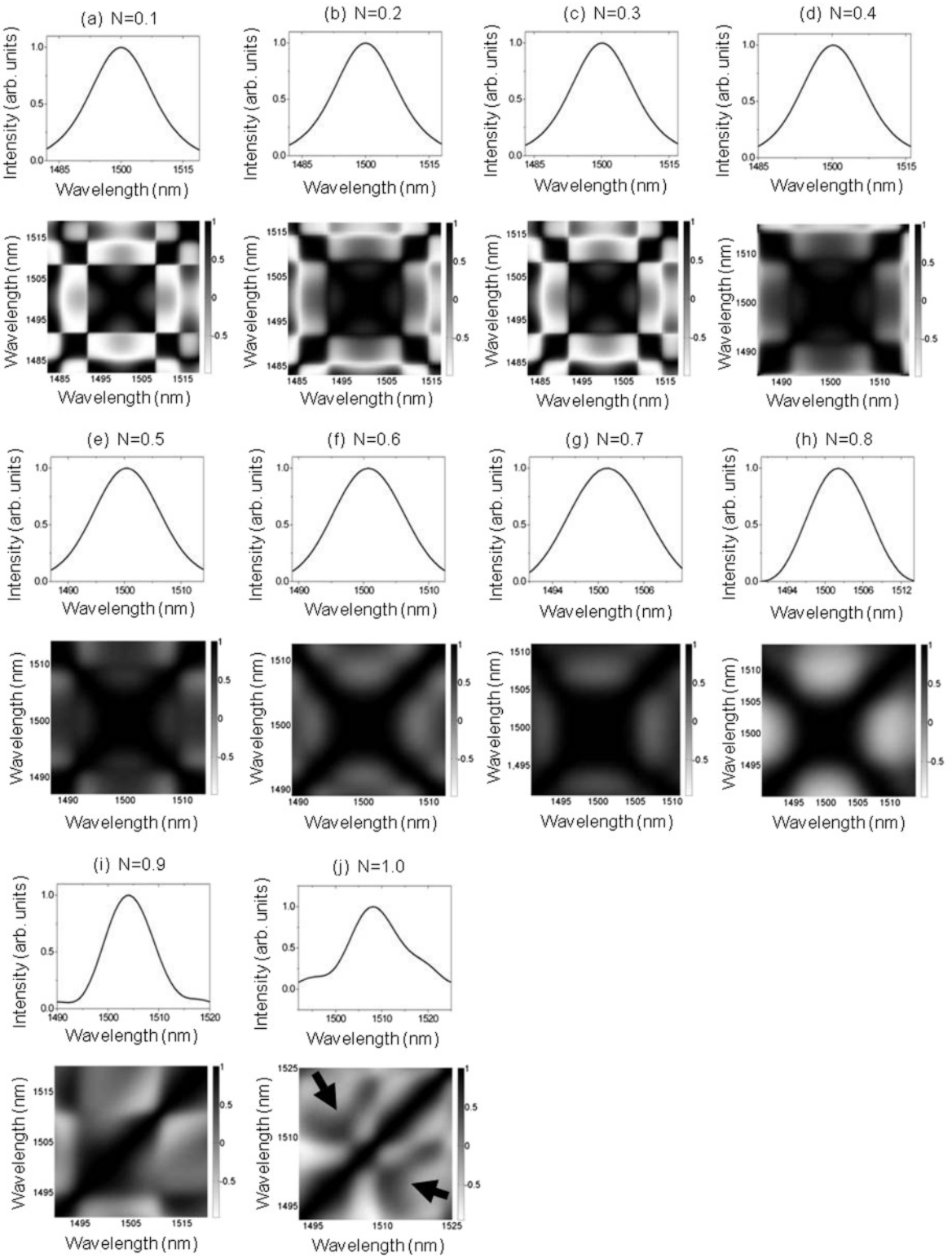


FIG. 2. Normalized quantum spectral correlation matrices (lower half of each figure) with the corresponding output pulse spectra (upper half of each figure) for soliton orders from $N = 0.1$ to $N = 1.0$.

and the white at $N = 0.5$, 0.6, and 0.7 is lower than that at $N < 0.4$, implying the further redistribution of correlations in the matrices. As depicted in Fig. 2(h), at $N = 0.8$, the X-shaped strong correlations become distinct while the strong anticorrelations are found around the X-shaped correlations and the relevant contrast becomes distinct in the matrix, compared to the cases of $N = 0.5$–0.7.

The center of the square-shaped correlation which is positioned at the pulse spectrum center at $N \leqslant 0.5$ shifts toward the shorter wavelength at $N = 0.6$–0.8, producing

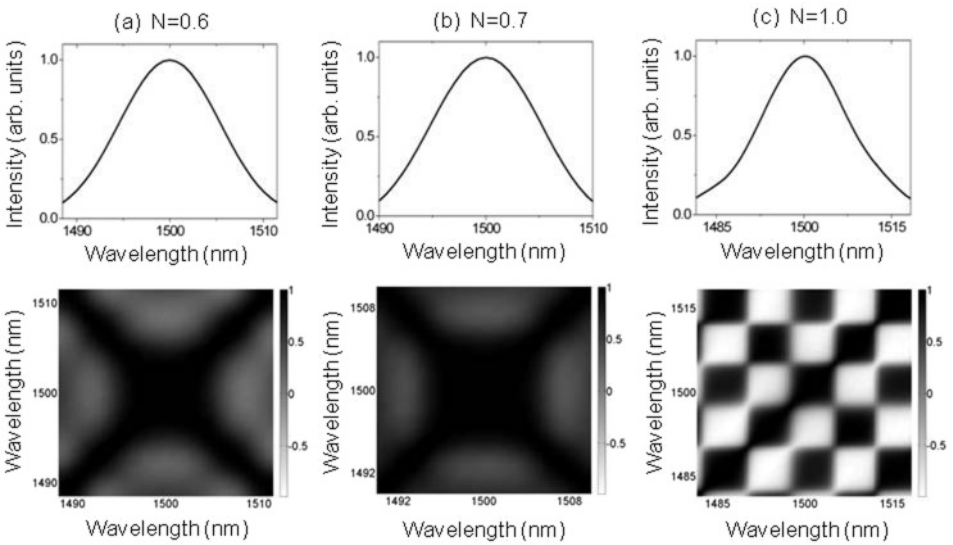


FIG. 3. Normalized quantum spectral correlation matrices (lower half of each figure) with the corresponding output pulse spectra (upper half of each figure) for soliton orders, $N = 0.6$, 0.7, and 1.0, based on the calculation with no terms related to the Raman scattering but all the other terms remaining.

the asymmetry of the pattern. With the spectrum narrowing, the shifted correlation square gets smaller at $N = 0.8$ than in the cases of $N \leqslant 0.4$. The asymmetric features of the quantum correlation matrices, which are accounted for by higher-order nonlinear effects such as intrapulse-stimulated Raman scattering, begin to be visible at $N = 0.6$ and become significant at $N \geqslant 0.7$, while the self-frequency shift of the pulse spectrum (classical evolution) becomes significant at $N \geqslant 0.9$. This implies that nonlinear effects such as intrapulse-stimulated Raman scattering, which are not detectable distinctly at the classical level, can be measured at the quantum level.

At $N = 0.9$, the anticorrelations in the matrix are extended toward the matrix centers, indicating the presence of strong anticorrelations between the spectrum wings and the center, as depicted in Fig. 2(i). At the soliton energy level [Fig. 2(j)], anticorrelations are further extended across the matrix while the strong correlations (diagonal shape) associated with the spectrum wings remain. The asymmetric pattern of the correlation matrix around the spectrum center becomes significant with $N$ approaching 1.0. At $N = 1.0$, the correlations associated with short- and long-wavelength spectrum wings (see arrows) are found in the asymmetric way, in addition to the outlying spectrum-wing-related strong correlations along the diagonal direction in the asymmetric way. This leads to the expectation that the removal of outlying spectral components produces photon-number squeezing, and short-wavelength pass filtering gives a higher degree of photon-number squeezing than can be obtained by long-wavelength pass filtering. This is qualitatively in agreement with the asymmetric squeezing degree for solitons [5,7].

For subsolitons near $N = 1.0$, asymmetry of the squeezing degree between a short-wavelength and a long-wavelength pass filtering can be expected from the asymmetric structure of the correlation matrices presented in Figs. 2(f)–2(i), being in qualitative agreement with the experimental results for subsolitons [15]. Anticorrelations that are found to extend toward the spectrum center in the correlation matrix as $N \to 1.0$ benefit the enhancement of photon-number squeezing by spectral filtering of outlying spectrum components with $N \to 1.0$. This is also qualitatively in agreement with the properties of photon-number squeezing obtained experimentally by spectral filtering of subsolitons, which also show degrees lower than those of soliton cases in an optical fiber [7,15].

For soliton orders from 0.1 to 1.0, quantum noise calculation is also performed with and without pulse-self-steepening-effects-related terms to check their exclusive effects on the quantum spectral correlation, and it is seen that the pulse-self-steepening effects are negligible compared to the other nonlinear effects discussed above.

Figures 3(a)–3(c) show the quantum spectral correlation matrices at $N = 0.6$, 0.7, and 1.0, which are calculated with no terms relevant to intrapulse-stimulated Raman scattering but with all the other terms remaining. Asymmetric properties disappear compared to the cases in Figs. 2(f), 2(g), and 2(j), as expected. It is also noted that, at $N = 1.0$, the intrapulse-stimulated Raman scattering redistributes quantum spectral correlations such that correlations of chessboardlike patterns in the matrix as shown in Fig. 3(c) are smeared into those as shown in Fig. 2(j).

Spontaneous Raman noise effects can influence quantum fluctuations [18,19]. However, their inclusion in the calculation is beyond the scope of our calculation framework which does not use a stochastic approach but only supports the calculation of quantum (vacuum) noise propagation along a fiber with the input condition of vacuum noise (unit matrix of $\mu_{pq}$ and zero matrix $\nu_{pq}$).

## IV. CONCLUSION

Intrapulse quantum spectral correlations of the femtosecond (130 fs) $\mathrm{sech}^2$ pulsed light of a soliton order $N \leqslant 1.0$ in an optical fiber is examined by calculating the quantum noise propagation. The calculation that includes SPM, GVD, and higher-order nonlinear effects, such as pulse self-steepening and intrapulse-stimulated Raman scattering, produces quantum spectral correlation matrices at soliton orders, including low orders, $N = 0.1$ to 1.0 (a 0.1 step), with a spectral resolution of 0.7 nm. This can be expected to give more detailed information on the quantum spectral correlations than the case of investigating the photon-number squeezing (variance) under a spectrally integrated passband filter [5,6]. The correlation

matrix evolves with the pulse energy (soliton order) under the nonlinear effects that are responsible for redistribution of correlation properties.

For all soliton orders used in the calculation, the pulse self-steepening effects turn out to be negligible compared to the other effects involved in the calculation. For low soliton orders, i.e., $N \leqslant 0.4$, major correlations are found between spectral components near the spectrum center, resulting in the square-shaped region of correlation in the matrix. At $N = 0.5$, the cross-shaped correlations in the matrix begin to be distinct, indicating that the phase transition of internal quantum noise structure occurs at around $N = 0.5$, as similarly found in Refs. [5,6]. It is also seen that asymmetric features in the correlation matrices begin to be visible at $N = 0.6$ while the self-frequency shift of the pulse spectrum (classical counterpart) becomes visible at $N = 0.8$. Under the increasing nonlinear effects as $N \rightarrow 1.0$, anticorrelations are, however, increasingly extended to be seen toward the spectrum center in the correlation matrices with the redistribution of correlations, subject to the conservation of total photon-number noise (variance) of the whole pulse spectrum. This leads to the expectation that the degree of photon-number squeezing by spectral filtering for the subsolitons will be lower than that for the fundamental soliton.

Intrapulse-stimulated Raman scattering is responsible for the asymmetric feature of the correlation matrices that results in the asymmetry of photon-number squeezing between a short-wavelength and a long-wavelength pass filtering of an optical pulse of a soliton order $N \leqslant 1.0$. In particular, the comparison made between correlation matrices calculated without and with the intrapulse-Raman-scattering-related terms at $N = 1.0$ shows that the Raman scattering redistributes the chessboardlike correlations in the matrix into the smeared pattern.

The evolution of correlation matrices with the pulse energy implies that nonlinear effects such as SPM and intrapulse-stimulated Raman scattering, which are not detectable distinctly at the classical level, can be detectable at the quantum level.

## ACKNOWLEDGMENT

This work was supported by the Gachon University Research Fund of 2012 (GCU-2011-R376).

[1] B. L. Schumaker, S. H. Perlmutter, R. M. Shelby, and M. D. Levenson, Phys. Rev. Lett. **58**, 357 (1987).
[2] M. D. Levenson and R. M. Shelby, J. Mod. Opt. **34**, 775 (1987).
[3] S. R. Friberg, S. Machida, M. J. Werner, A. Levanon, and T. Mukai, Phys. Rev. Lett. **77**, 3775 (1996).
[4] A. Sizmann, Appl. Phys. B **65**, 745 (1997).
[5] S. Spälter, M. Burk, U. Strössner, M. Böhm, A. Sizmann, and G. Leuchs, Europhys. Lett. **38**, 335 (1997).
[6] M. J. Werner and S. R. Friberg, Phys. Rev. Lett. **79**, 4143 (1997).
[7] S. Spälter, M. Burk, U. Strössner, A. Sizmann, and G. Leuchs, Opt. Express **2**, 77 (1998).
[8] S. Spälter, N. Korolkova, F. König, A. Sizmann, and G. Leuchs, Phys. Rev. Lett. **81**, 786 (1998).
[9] S. J. Carter and P. D. Drummond, Phys. Rev. Lett. **67**, 3757 (1991).
[10] M. J. Werner, Phys. Rev. A **60**, R781 (1999).
[11] K. Hirosawa, H. Furumochi, A. Tada, F. Kannari, M. Takeoka, and M. Sasaki, Phys. Rev. Lett. **94**, 203601 (2005).
[12] A. Tada, K. Hirosawa, F. Kannari, M. Takeoka, and M. Sasaki, J. Opt. Soc. Am. B **24**, 691 (2007).
[13] C. R. Doerr, M. Shirasaki, and F. I. Khatri, J. Opt. Soc. Am. B **11**, 143 (1994).
[14] N. Nishizawa, T. Horio, M. Mori, T. Goto, and K. Yamane, Jpn. J. Appl. Phys. **38**, 1961 (1999).
[15] H. Ju, D.Phil. thesis, University of Oxford, 2002.
[16] G. P. Agrawal, *Nonlinear Fiber Optics*, 3rd ed. (Academic Press, San Diego, 2001).
[17] R. Q. Hui, O'Sullivan, A. Robinson, and M. Taylor, J. Lightwave Technol. **15**, 1071 (1997).
[18] P. D. Drummond and J. F. Corney, J. Opt. Soc. Am. B **18**, 139 (2001).
[19] J. F. Corney, J. Heersink, R. Dong, V. Josse, P. D. Drummond, G. Leuchs, and U. L. Andersen, Phys. Rev. A **78**, 023831 (2008).